ACS APPLIED MATERIALS & INTERFACES
Research Article
www.acsami.org

Synergistic Effect of pH and Phase in a Nanocrystalline Titania Photocatalyst

Nichola M. Kinsinger, Alexander Dudchenko, Ashley Wong, and David Kisailus*

Department of Chemical and Environmental Engineering, University of California, Riverside, California 92521, United States

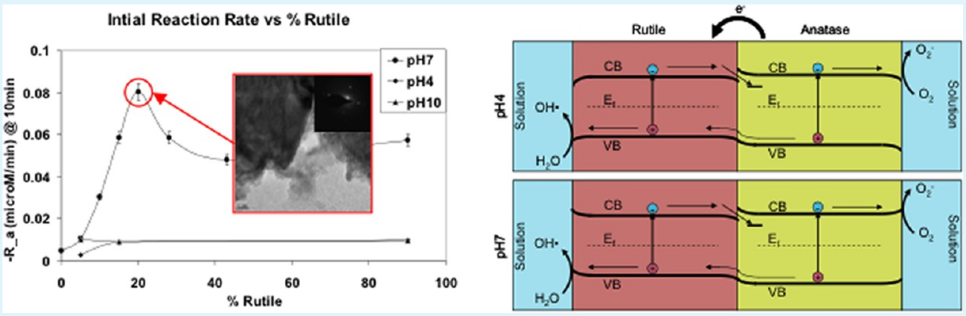

ABSTRACT: Titanium dioxide is a semiconducting material that has been studied for many years as a photocatalytic material to degrade organics in water. This study investigated the effect of anatase-rutile mixtures and pH on the photocatalytic degradation of the dye Methylene blue as the target analyte. Anatase-rutile mixtures between 0 and 90% rutile that were synthesized from a water-soluble precursor were suspended at pH 4, 7, and 10. Suspension pH significantly affected the reactivity and efficiency of the photocatalysts because of the particle−particle and sorbate−surface interactions. The highest removal percentage of MB by 240 min at pH 4, 7, and 10 was 35, 99, and 93%, respectively. pH 7 was ideal to observe the affect of percent rutile on the degradation rate, where 91% was removed within 120 min by the material composed of 20% rutile, which is attributed to the synergistic charge transfer of holes from rutile to anatase.

KEYWORDS: *TiO_2, titania, hydrothermal, anatase-rutile, photocatalysis*

1. INTRODUCTION

The rapid increase in production of industrial chemicals and pharmaceuticals and their discharge into the wastewater system presents multiple issues, such as interference with hormone regulatory systems and reproductive damage to humans and wildlife.[1,2] The occurrences of emerging contaminants now being detected, along with the advancement in measurement technologies, are causing increased concern for public health and safety.[3−7] Pharmaceuticals and personal care products (PPCPs), surfactants, and various industrial chemicals are known to be endocrine disrupting compounds (EDCs).

The use of wastewater effluents to augment water supplies in areas of water scarcity increases the likelihood of such contaminants (pharmaceuticals) occurring in drinking water.[3,6] Alarmingly, one study detected a combination of 11−17 different organics in finished water from a drinking water treatment facility.[6] Degradation of organic compounds via oxidation by photocatalytically induced hydroxyl radicals (OH●) is a potential treatment technology that can degrade a wide range of organic compounds to complete mineralization with no selectivity.[6,8−14]

Titanium dioxide (TiO_2) is of significant interest because of its semiconducting properties that enable its use as a heterogeneous photocatalytic material, rapidly and completely mineralizing organic compounds in water when exposed to UV irradiation without harmful byproducts.[8,9] Light with energy greater than the band gap can generate electron−hole pairs. The charge vacancy (hole, h^+) left in the valence band by the excited electron oxidizes adsorbed water producing hydroxyl radicals.[9,13,15−17]

Anatase and rutile are the two photocatalytically relevant phases of TiO_2 with bandgaps of 3.2 and 3.0 eV, respectively.[18−21] Anatase, a metastable phase, has been shown to be more photocatalytically active than the thermodynamically stable rutile phase, which is the stronger photoabsorber. Mixed phase TiO_2 (i.e., anatase and rutile), such as Degussa P25 (an industrially produced photocatalyst), has been shown to be more effective than either pure anatase or rutile phase TiO_2.[18,19] The improved performance of this mixed phase photocatalyst is attributed to a synergistic charge transfer across the anatase-rutile interface.[18,19,22] Although the mechanism of electron transfer between the different phases (anatase and rutile) is not clearly understood, it is evident that the presence of both phases greatly improves the photocatalytic activity.[18] However, the proportions of these phases required for optimum photocatalytic activity is debatable because of the differences in synthesis processes, crystallite sizes, and interactions between phases. However, these studies did not

Received: April 6, 2013
Accepted: June 14, 2013
Published: June 14, 2013

dx.doi.org/10.1021/am401247h | ACS Appl. Mater. Interfaces 2013, 5, 6247−6254

address the impact of particle−particle and sorbate−surface interactions that depend on the pH at which photocatalytic reactions are performed.

Operating parameters such as pH have been reported to greatly affect heterogeneous photocatalytic performance due to particle aggregation, which will reduce accessible surface active sites and block excitation events within the catalyst.[23] The pH also affects the ionization state of catalyst surface and the organic compounds, which has been shown to affect the sorbate−surface interactions that impact performance due to scavenging of OH● radicals.[24−30]

Thus, we investigate the effects of TiO_2 phase and suspension conditions using TiO_2 synthesized using a water-soluble and stable precursor[31] in order to reveal the optimum conditions for the photocatalytic degradation of methylene blue (MB), a common analyte used in determining photocatalytic reaction rates.

2. EXPERIMENTAL SECTION

2.1. Preparation of Materials. TiO_2 photocatalytic materials were synthesized under hydrothermal conditions. Briefly, 1 M Titanium bis(ammonium lactato) dihydroxide (TiBALDH, Sigma Aldrich) solutions were prepared by diluting with deionized (DI) water. After dilution, ammonium hydroxide (30 wt %, Acros Organics) was used to adjust the solution pH to ∼9. The solutions were placed in Teflon-lined steel reactors (Parr Instruments, Moline, IL) at 150 °C for different durations (1−72 h). The resulting products were centrifuged, washed with DI water, sonicated (Branson 2510) for 30 min between washes (to remove any unreacted precursor and reaction byproducts) and subsequently dried in air at 100 °C for 24 h.[31]

2.2. Material Characterization. TiO_2 powders were characterized using X-ray diffraction (XRD), Transmission Electron Microscopy (TEM), Surface area analysis via the Brunauer, Emmett, and Teller (BET) method, and Zeta Potential measurements. The resulting phases were determined by X-ray Diffraction (XRD) analysis (Philips X'Pert) using Cu Kα radiation. Crystallite diameters of anatase and rutile crystals were calculated based on the (200) and (210) reflections, respectively, using the Scherer formula (eq 1)

$$D_{(hkl)} = \frac{\kappa\lambda}{\beta\cos\theta} \tag{1}$$

where κ is the shape factor, λ the wavelength of the Cu Kα radiation, β the full width at half-maximum (fwhm) of the (h k l) peak, and θ is the diffraction angle. The relative composition of crystalline rutile was determined via the following equation (eq 2)

$$x_r = \frac{I_R}{I_R + 0.884 I_A} \tag{2}$$

where I_A and I_R are the integrated intensities of anatase (101) and rutile (110) peaks, respectively.[32] In order to corroborate these results, specimens were observed using both bright field imaging and electron diffraction analyses in TEM (T-12, T-20, and Titan, FEI). TiO_2 nanocrystals were dispersed in ethanol, sonicated (Branson 2510) for 30 min, and subsequently deposited onto ultrathin carbon films on holey carbon supports with a 400 mesh copper grid (Ted Pella).

The surface areas of powders were determined via BET nitrogen adsorption at 77K using a Micromeritics Tristar 3000. Prior to analysis, samples (∼100 mg) were degassed at 90 °C for 6 h under a vacuum. The adsorption isotherms of nitrogen at 77 K were obtained using fifteen relative pressure values ranging from 0.05 to 0.35.

Zeta potential analysis was used to characterize the surface charge and isoelectric point (IEP) of the as-synthesized materials. Suspensions (500 mg/L) of TiO_2 nanomaterials (UV pretreated for 24 h prior to characterization) were prepared incrementally from pH 3 to pH 10 by the addition of hydrochloric acid and ammonium hydroxide in a 0.01 M sodium chloride solution. The zeta potential was measured using ZetaPALS analyzer (Brookhaven Instruments Corp. Holtsville, NY).

2.3. Photocatalytic Performance. The effects of suspension pH and anatase-rutile ratios on photocatalytic activity were determined by measuring the degradation of Methylene Blue (MB) in the presence of TiO_2 nanoparticle suspensions under UV illumination. Prior to degradation testing, TiO_2 suspensions were prepared by dispersing the TiO_2 powders in filtered deionized water (0.22 μm, Millipore), adjusting the pH to either 4, 7, or 10 with hydrochloric acid or ammonium hydroxide, respectively, and sonicating for 5 min using a tip-horn ultrasonic processor (Hielscher UP100H, Ringwood, NJ). Any residual organics remaining on the surface of the TiO_2 photocatalytic material (i.e., from the synthesis process) were removed by irradiating the material for 24 h prior to testing with UV light (Phillips UV (A) 40 W bulb at $1 mW/cm^2$). Fourier Transform Infrared Spectroscopy (FTIR) was used to confirm the absence of residual organic (data not shown).

In a typical degradation reaction, a glass reactor was filled with 100 mL containing (i) a 500 mg/L TiO_2 suspension and (ii) 13 μM solution of Methylene Blue (MB) maintained at 25 °C and magnetically stirred at 500 rpm. The photon source was a Phillips UV (A) 40 W bulb operated at $1 mW/cm^2$. At the start of each degradation experiment, MB (under dark conditions) was allowed to absorb onto the suspended TiO_2 for one hour prior to irradiation, followed by direct irradiation with the photon source. The photocatalytic activity was monitored by measuring the absorbance of MB via UV−visible Spectroscopy (Beckman Coulter DU 800 Spectrophotometer) between 200 and 800 nm (λ_{max} = 668 nm).

Reaction rates were determined by fitting the MB degradation over time with pseudofirst order equation:

$$C_t = C_o e^{-kt} \tag{3}$$

where C_t is the concentration of MB in solution at time t, C_o is the initial concentration of MB in solution, and k is the pseudo-first-order rate constant.

Additional photocatalytic experiments were conducted using platinum (Pt) deposition via photocatalytic reduction of ammonium hexachloroplatinate (NH_4PtCl_6) to characterize the location (i.e., anatase, rutile, or both phases) of the reduction half of the photocatalytic reaction that occurs on the mixed phase photocatalytic materials. 0.1 mM (NH_4PtCl_6) solutions were prepared using deionized water and adjusting to the desired pH using ammonium hydroxide or hydrochloric acid.[33] During the Pt deposition reaction, the suspensions were maintained at 25 °C under an anaerobic atmosphere and magnetically stirred at 500 rpm.

3. RESULTS AND DISCUSSION

3.1. Material Characterization. To investigate the effects of phase on the photocatalytic degradation, mixed phase TiO_2 samples were prepared by adjusting the hydrothermal reaction parameters (primarily time).[31] The relative phase composition (i.e., rutile and anatase) for products at each duration were determined using eq 2 and are depicted in Figure 1. At short reaction times (i.e., 1 h), nanosized (3.1 ± 0.1 nm) anatase (JCPDS # 01−084−1286) is the primary phase observed (Figure 1a). Larger rutile (JCPDS #01−073−1765) crystals (14.4 ± 4.1 nm) are clearly present (via XRD measurements) after 12 h and continue to grow at the expense of the anatase crystals via oriented attachment.[31] The anatase crystallite size increases slightly from 3.1 ± 0.1 nm (1 h) to 5.1 ± 0.2 nm after 72 h. Complete transformation to rutile occurs by 72 h with significantly larger rutile crystallites formed (32.1 ± 6.9 nm). TEM analysis of the resulting nanoparticles (Figure 1b) confirms the presence of the mixture of phases at different times. In addition, the crystallite sizes of anatase observed in TEM are consistent with XRD measurements. However, TEM micrographs reveal much larger (72 ± 11 nm diameter × 141 ±

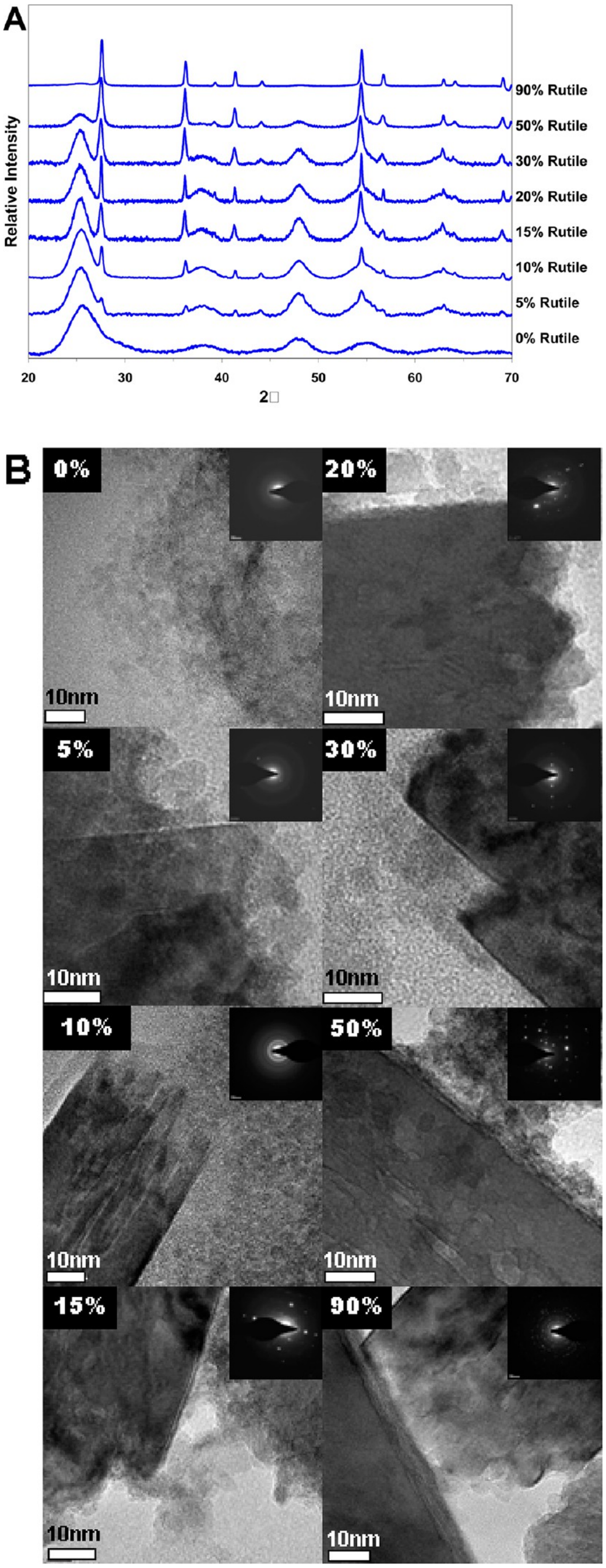

Figure 1. (A) X-ray diffraction patterns and (B) bright-field TEM micrographs (with selected area diffraction patterns inserted) of mixed phase TiO_2 (anatase/rutile) formed hydrothermally at pH 9, 150 °C at different times.

27 nm long) rod-like rutile crystals that are coated with anatase crystallites. Discontinuous segments and twists within one rod-like rutile particle are observed in the TEM micrographs due to the attachment of the smaller anatase crystallites. Consistent with an oriented attachment growth mode, the larger secondary rutile particle is composed of primary particles (i.e., crystallites) that are assembled to form the rodlike particles that have slight discontinuities between these primary crystals, as confirmed via XRD.[31,34,35]

BET surface area analyses (Table 1) of the mixed phase TiO_2 reveals a decrease in surface area with increasing rutile content, in agreement with the observation of the larger rutile crystals seen in Figure 1b.

Table 1. Surface Area vs. Percentage of Rutile

rutile percentage (%)	surface area (m^2/g)
0	277.3 ± 2.8
5	281.9 ± 9.84
10	284.7 ± 4.60
15	272.9 ± 1.36
20	278.9 ± 1.60
30	273.4 ± 7.83
50	205.4 ± 1.7
90	44.2 ± 1.1

The surface charge of colloids has a significant effect on their aggregation behavior.[27] In order to assess the effect of dispersion on the photocatalytic activity of TiO_2 suspensions, the pH was adjusted with subsequent investigation of colloidal behavior. TiO_2 suspensions prepared at different pHs were subjected to zeta potential measurements. The isoelectric points (IEPs) of our synthesized TiO_2 were observed (Figure 2) to be at lower pH values compared to other TiO_2 materials reported (pH ~6).[27,36−38] The IEP of pure anatase TiO_2 was measured at pH 4.5. However, with increasing concentration of rutile, the IEP shifts to higher pH values, with the IEP of a 90% rutile−10% anatase TiO_2 measured at pH 5.7. The shift in IEP is likely attributed to the increasing concentration of rutile crystals, which display (110) surfaces (as observed in TEM). These surfaces have been reported to have an IEP at pH 5.5.[39] In addition, the IEP shift may be related, in part, to the reduced acidity of the materials resulting from the reduced total surface area.[27] Anatase-rich samples suspended at pH 4 are comprised

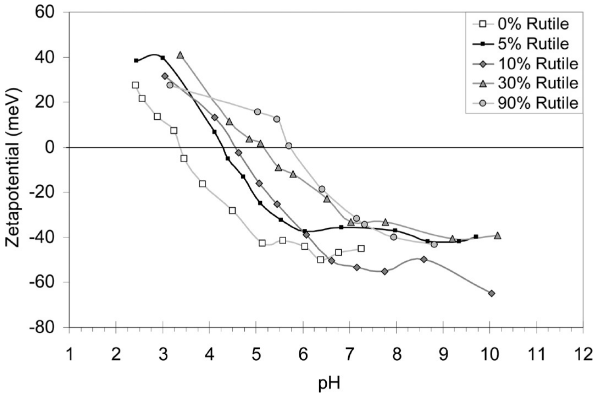

Figure 2. Zeta potential curves of the mixed phase TiO_2 nanoparticles with increasing relative rutile concentration, suspended in 0.01 M NaCl solution.

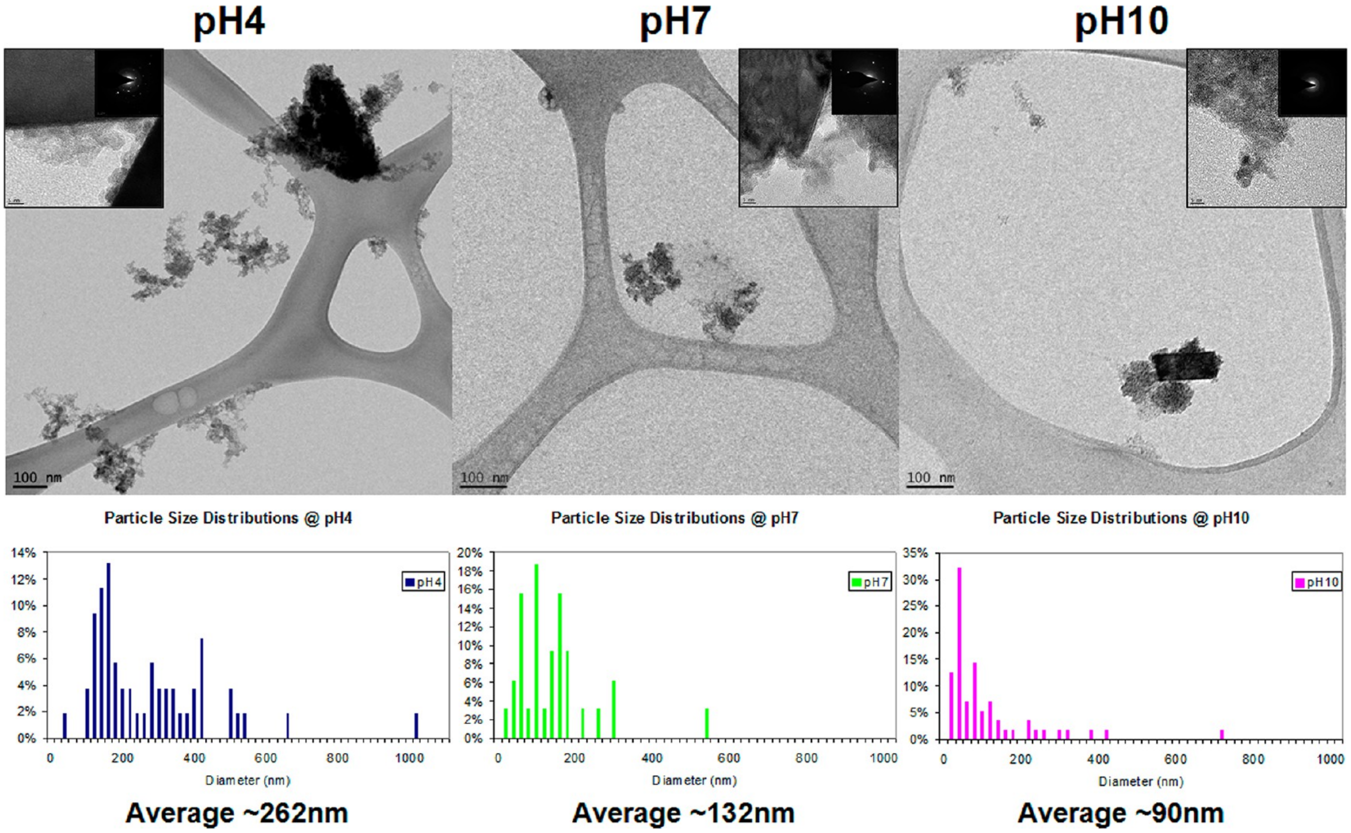

Figure 3. Bright-field TEM micrographs of 80% anatase−20% rutile TiO_2 materials suspended at (a) pH 4, (b) pH 7, and (c) pH 10 with subsequent particle size distributions. TEM specimens were prepared by suspending the TiO_2 in water at the specified pH, sonicating for 5 min, and placing a small drop (10 μL) onto a TEM grid. 50 particles were measured per sample.

of larger aggregates, a result of a relatively weak positive surface charge (i.e., approximately +10 mV for both 92 and 88% anatase-based samples). However, anatase-rich TiO_2 suspensions prepared at pH 7 or 10 were significantly charged (i.e., greater than −20 mV) and were thus well-dispersed due to strong interparticle electrostatic repulsion.

TEM micrographs of particle suspensions prepared at pH 4, 7, and 10 (Figure 3) were obtained to characterize their dispersivity. Large aggregates (ca. 300 nm) form at pH 4 due to the weak interparticle forces. As expected, suspending these particles at pH 7 leads to an increase in surface charge (>20 mV) with a subsequent reduction in aggregate size (ca. 130 nm) and a further reduction (ca. 90 nm) at pH 10. Since materials suspended at pH 4 were near the IEP, they rapidly aggregated and settled in suspensions that were not stable for the duration of the Dynamic Light Scattering (DLS) measurements (unlike the materials suspended at pH 7 and 10). This aggregation significantly reduces the accessible surface area while increasing the effective stokes radius, which leads to settling. The average particle sizes measured using DLS at pH 4, 7, and 10 were 1037.0 ± 208.1 nm, 105.3 ± 13.0 nm, and 95.1 ± 4.4 nm, respectively. Therefore, we also prepared TEM specimens to characterize these suspensions (pH 4, 7, and 10). The stable suspensions at pH 7 and 10 yielded consistent average particle sizes between TEM and DLS characterization methods, but not for pH 4, which is attributed to the delay in sampling using DLS as compared to TEM samples.

3.2. Kinetics of Photocatalytic Degradation: Effect of pH and Anatase−Rutile Ratio.

Methylene blue (MB), a compound used for therapeutic treatments of methemoglobinemia, ifosfamide-induced encephalopathy, and cyanide poisoning[40,41] is also a commonly used analyte for photocatalytic degradation studies, and was subsequently chosen as the model pollutant to test the activity of synthesized photocatalytic materials.[28,42−44]

3.2.1. Effect of Suspension pH. Suspension pH had a dramatic effect on the reactivity and efficiency of the photocatalysts due to the particle−particle and sorbate-surface interactions. The highest removal percentage of MB by 240 min at pH 4, 7, and 10 was 35, 99, and 93%, respectively, with 91% removed within 120 min by materials composed of 20% rutile suspended at pH 7. When irradiated with UV (A) light in the absence of the TiO_2 catalyst, no obvious degradation of MB was observed; therefore, direct photolysis was negligible at all experimental conditions considered.

pH is observed to be a major factor influencing both the rate and mode of degradation. The reduced efficiency observed at pH 4 may, in part, be attributed to the increase in aggregation (vs other pH conditions, Figure 3). Aggregation reduces the accessible surface available for analyte adsorption and photocatalytic reactions. In addition, large aggregates (diameter ~1 μm) lead to shadowing of internal crystals from incoming photons and will thus experience fewer excitation events, reducing photocatalytic activity.[23] Minimal dye adsorption on TiO_2 materials suspended at pH 4 (Figure 4a) may also attribute to the reduced efficiency. MB is a cationic dye, which will be electrostatically repelled by the positive charge of the catalyst surface under acidic (i.e., TiO_2 at pH 4) conditions.[26,28−30] Thus, there is an increase in the diffusion time of the OH● from reduced sorbate−surface interactions and

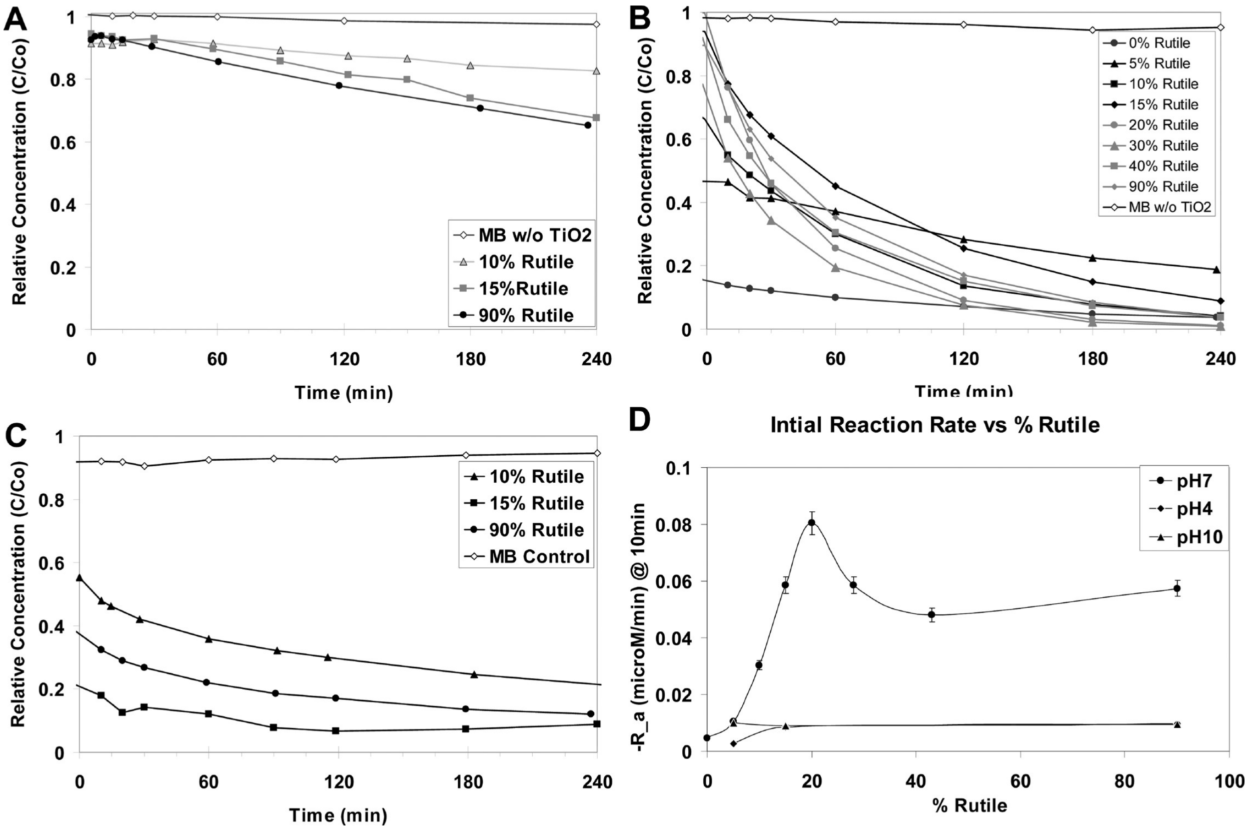

Figure 4. Photocatalytic degradation of MB versus time. Reactions were performed using TiO_2 suspensions (500 mg/L TiO_2, 1 mW/cm^2 UV light intensity) at (A) pH 4, (B) pH 7, (C) pH 10. (D) Initial degradation rate of MB versus % rutile in TiO_2 suspensions at pH 4, 7, and 10 (lines drawn only as a guide).

therefore increases the likelihood of the radical being scavenged.

Conversely, under more alkaline conditions, where the photocatalyst is negatively charged (Figure 2), adsorption of MB is favorable. However, absorption does not account for a signification proportion of removal at pH 7 (Figure 4b), whereas at pH 10, absorption is observed to be the major source of dye removal because of the increasing surface charge of the photocatalyst material.[45] Photocatalytic activity is enhanced due to proximity of dye to oxidation species, allowing for direct hole oxidation. Considerable absorption of MB on the catalyst surface obstructs the diffusion of electron scavengers such as dissolved oxygen to the surface. In fact, several layers of MB absorbed on the surface may block excitation of the photocatalytic reaction, thus hindering photocatalytic activity as seen in Figure 4.[24,25]

3.2.2. Effect of Anatase–Rutile Ratio. The degradation efficiency of the mixed phase TiO_2 suspensions was observed to be pH dependent. The observed reaction rates (at 10 min) versus percent rutile at all three pH conditions (i.e., pH 4, 7, 10) are illustrated in Figure 4d. Degradation rates of materials suspended at pH 4 improve with increasing rutile content. However, these reaction rates are still lower than those at pH 7, with 20% rutile achieving the highest removal rates. At pH 4, increasing the rutile content produces a more stable suspension due to increased surface charge (>20 meV). The result is a less aggregated suspension, which reduces the shadowing effect.[23] As discussed previously, the highest degradation rate was observed at pH 7 with a 20% rutile–80% anatase phase mixture of TiO_2, which is consistent with previous studies.[46] This is indicative of a synergistic effect between anatase and rutile interfaces, where contact is necessary, rather than a combination of the individual photocatalytic properties.[22]

The effect of crystal size on the photocatalytic behavior is negligible. Although TEM observations show changes in anatase crystal sizes between 3.1 ± 0.1 nm (0% rutile) and 5.1 ± 0.2 nm (90% rutile), there are very small changes in crystal sizes in the region of greatest photocatalytic activity change (i.e., 10 − 30% rutile). Within this range, the anatase crystal sizes increase slightly from 4.1 ± 0.1 nm to 4.3 ± 0.2 nm, whereas the increase in the primary rutile crystallites size is minimal (from 14.4 ± 4.1 nm to 22.9 ± 4.5 nm, as measured via XRD).

Although several studies[22,47−50] have observed size effects on photocatalytic performance of TiO_2 such as an increase in the observed bandgap in crystals smaller than 10 nm (the reported sizes vary from 2 to 20 nm), we do not observe this with our 4 nm anatase crystals. In these small anatase crystals, the depletion region and the surface band bending is likely to be minimal compared to that observed in rutile (the band bending in Figure 5 is not drawn to scale).[47] However, this effect may contribute to the photocatalytic activity because the minimal upward band bending in anatase will be more favorable for electron transfer to oxygen compared to more crystalline materials, which may have significant upward bending, which is unfavorable for electron transfer.[21,47,48]

Several studies have reported enhanced photocatalytic performance with anatase–rutile mixtures due to a perceived synergistic mechanism between the anatase and rutile crystals.[18,46,49−51] If anatase and rutile crystals are in contact,

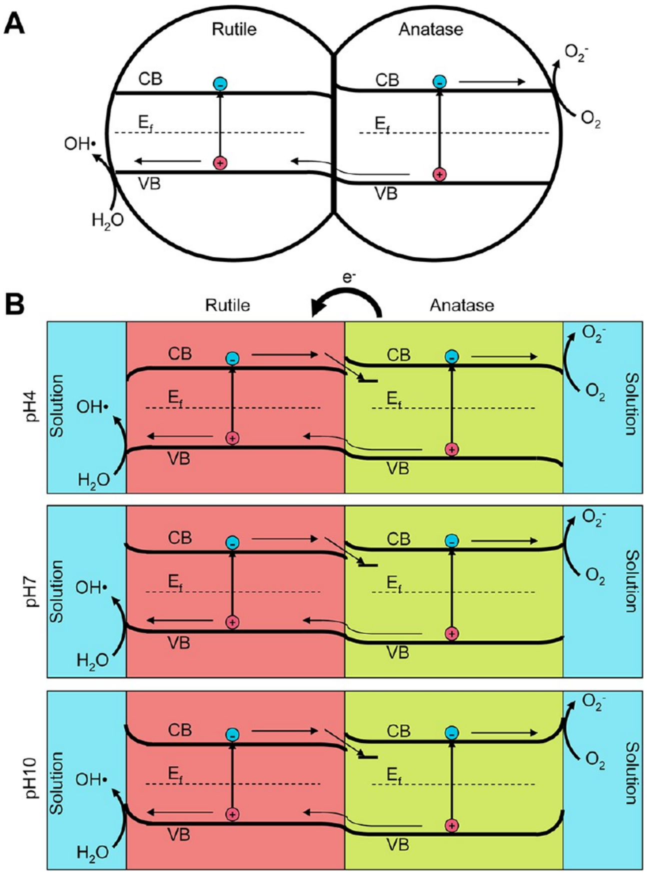

Figure 5. (A) Proposed mechanism of charge separation between anatase and rutile during photocatalysis. (B) Proposed mechanism of charge separation between anatase and rutile during photocatalysis at different suspension pHs on charge transfer to oxidation and reduction species.

electrons will transfer from anatase (higher Fermi level) to the rutile (lower Fermi level) until the Fermi levels in each crystal are equal.[21,47,52] Once equilibrium is reached, a space-charge region is formed because of the accumulation of electrons on the rutile crystals and a depletion region on the anatase crystals. This results in an upward band-bending in anatase and a downward band-bending in rutile (illustrated in Figure 5a). The presence of a space-charge layer at the surface of the particles will move the charge carriers in opposite directions and will favor the transfer of holes from anatase to rutile. The space-charge layer effectively reduces electron−hole recombination.[21,47,49,52] Because of the relatively small energy difference, it is possible (although unlikely) that electrons may transfer to anatase via thermal activation. In addition, electrons may transfer to anatase due to electron trap sites, which have been reported to be more stable than rutile.[18,22] Excited electrons on anatase can be readily scavenged by O_2 (the primary electron acceptor) since anatase has been reported to have a higher affinity for O_2 than rutile.[50] This will consequently enhance the oxygen reduction half reaction rate, which is typically the rate determining step and thereby reduce the electron−hole recombination.[53]

There are conflicting findings which report an optimal photocatalytic performance at different anatase-rutile ratios.[18,22,46,49−51,54,55] Some studies have indicated that more crystalline materials are more photocatalytically efficient and that specific facets of anatase are more active than others.[56] Surface states will change with differing synthesis conditions. Since there are multiple types of surface states, there are also multiple trap-to-band transitions with different energy levels that would affect the efficiencies of anatase and rutile,[50] which are prepared in different methods. Thus, it is highly likely that the resulting optimal ratio of anatase to rutile for photocatalysis is dependent upon sample preparation conditions.[18,56] Smaller anatase crystallites may result in a reduced photocatalytic efficiency versus rutile and mixed phase materials that contain more crystalline anatase.[57] Conversely, it has been shown that ultrafine TiO_2 particles have increased contents of surface Ti^{3+} as well as active Ti−OH species, which can enhance the photocatalytic activity of the TiO_2.[58] Anatase is observed to carry out the reduction half of the photocatalytic reaction which is the rate limiting step.[46,47,53] Therefore, a higher loading of anatase (vs rutile) may be necessary. Other effects may also dictate the optimal anatase-rutile ratio. These include surface defects formed from different process conditions that have been shown to have a significant effect on photocatalytic activity,[59] and may effect anatase−rutile interactions.[51]

The pH of the solution does not affect the potential difference between the band edges of anatase and rutile since they are in the same solution. However, it does effect the oxidation and reduction reactions that take place on the surface.[21,48] The positive surface charge at pH 4 creates an accumulation region at the solution−solid interface, which is unfavorable for hole transfer to the solution. However, it does facilitate electron transfer on anatase (as illustrated in Figure 5b). At pH 7 and 10, the negative surface charge creates a depletion region, which facilitates hole transfer while hindering the electron transfer.

At pH 4, where MB is not readily adsorbed onto the catalyst surface, degradation is presumably achieved solely via OH• oxidation. Despite the possible enhancement of electron transport across the solution−solid interface at the lower pH, the substrate−surface interaction dominated the photocatalytic degradation of MB.

Platinum (Pt) deposition via photocatalytic reduction of ammonium hexachloroplatinate (NH_4PtCl_6) was used to characterize the location (i.e., anatase, rutile, or both phases) of the reduction half of the photocatalytic reaction that occurs on the mixed phase photocatalytic materials. UV pretreated powders (12% rutile, which was observed to have the highest dye removal rate at pH 7) as described above were dispersed in the prepared solutions.

The photocatalytic reduction of Pt (IV) to Pt (0) resulted in the subsequent deposition of Pt nanoparticles on the surface of the catalyst.[33] The presence of multiple small Pt nanocrystals (~2 nm) was observed on the small anatase crystals surrounding large rutile crystals shown in Figure 6. Conversely, no Pt nanoparticle deposition was observed under the same conditions at pH 4. In addition, no Pt nanocrystals were observed on rutile crystals under any pH condition (i.e., pH 4 or 7). The Pt deposition occurs via reduction by excited electrons from the conduction band. This indicates that the reduction reaction is occurring predominantly on the anatase crystals and not on the large rutile crystals. This supports a synergistic mechanism, where a hole generated in anatase transfers to rutile. The hole transfer results in excess electrons in anatase promoting the reduction half reaction and excess holes in rutile promoting the oxidation half reaction. The lack of Pt nanocrystals deposition on TiO_2 suspensions at pH 4 is potentially due to the repulsion of the positively charged Pt ion

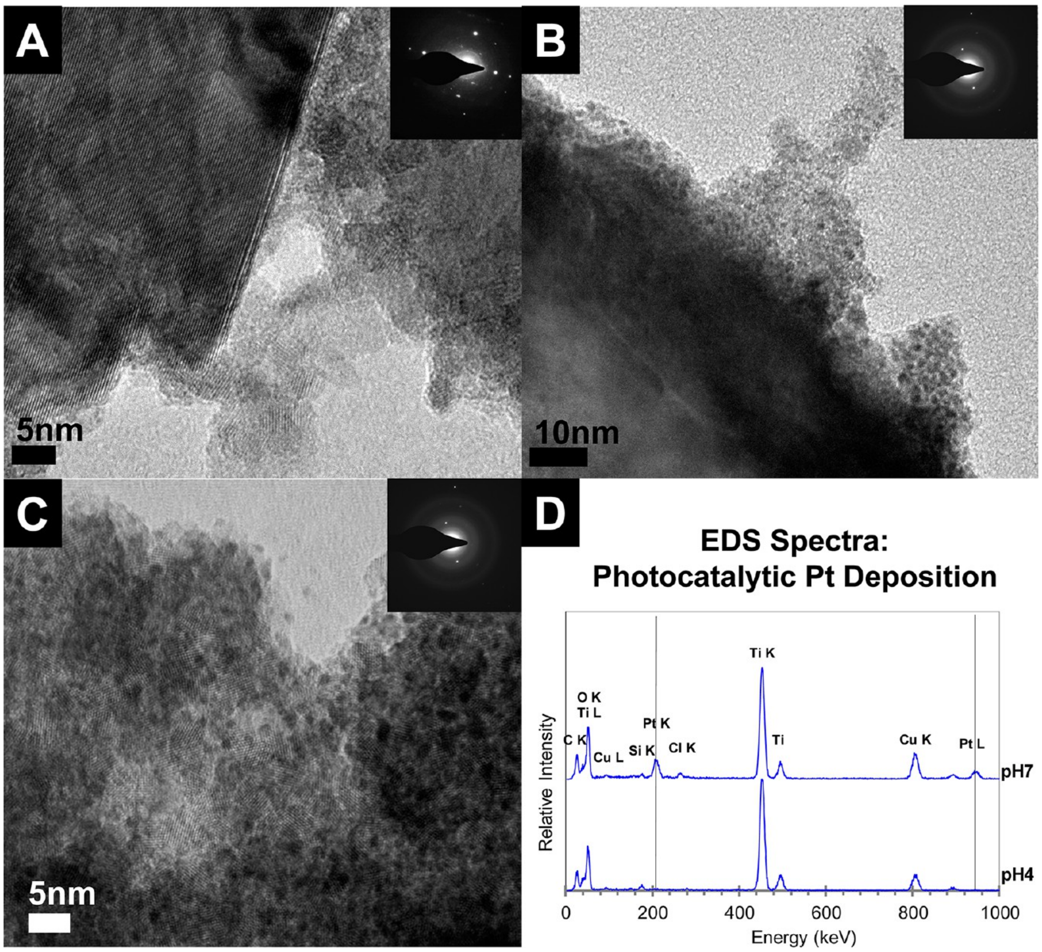

Figure 6. (a) Bright-field TEM micrograph of TiO_2 particles without Pt nanocrystal deposition, Pt deposition on 12% rutile material for 6 h at pH 7. (b) Low- and (c) high-magnification TEM images. (d) Energy-dispersive spectra of photocatalyst materials post Pt deposition at pH 4 (TEM image not shown) and pH 7. Selected area electron diffraction patterns are inserted for phase identification. EDS spectra are representative spectra from five regions samples.

by the positively charged TiO_2 surface similar to that observed with MB.

4. CONCLUSIONS

The suspension pH proved to significantly affect the photocatalytic activity of the material due to reduced proximity of oxidative species to the analyte under acidic conditions and increased proximity under alkaline conditions. pH 7 was the optimal reaction condition used to characterize the effect of anatase−rutile ratios on the photocatalytic activity. We observed an optimal ratio of 20% rutile−80% anatase at pH 7, which is attributed to the charge transfer of holes from rutile to anatase. This hole transfer results in excess electrons in anatase promoting the reduction half reaction and excess holes in rutile promoting the oxidation half reaction.

AUTHOR INFORMATION

Corresponding Author

*Address: B357 Bourns Hall, University of California, Riverside, CA 92521. Tel: 951.827.2260. Fax: 951.827.5696. E-mail: david@engr.ucr.edu. Web: http://www.engr.ucr.edu/~david/.

Notes

The authors declare no competing financial interest.

ACKNOWLEDGMENTS

This work was conducted with Government support under and awarded by DoD, Office of Naval Research, National Defense Science and Engineering Graduate (NDSEG) Fellowship, 32 CFR 168a.

REFERENCES

(1) Sharma, V. K. *Chemosphere* **2008**, *73* (9), 1379−1386.

(2) Chen, J. S.; Liu, M. C.; Zhang, L.; Zhang, J. D.; Jin, L. T. *Water Res.* **2003**, *37* (16), 3815−3820.

(3) Khetan, S. K.; Collins, T. J. *Chem. Rev.* **2007**, *107* (6), 2319−2364.

(4) Bolong, N.; Ismail, A. F.; Salim, M. R.; Matsuura, T. *Desalination* **2009**, *239* (1−3), 229−246.

(5) Petrovic, M.; Eljarrat, E.; de Alda, M. J. L.; Barcelo, D. *Anal. Bioanal. Chem.* **2004**, *378* (3), 549−562.

(6) Stackelberg, P. E.; Furlong, E. T.; Meyer, M. T.; Zaugg, S. D.; Henderson, A. K.; Reissman, D. B. *Sci. Total Environ.* **2004**, *329* (1−3), 99−113.

(7) Westerhoff, P.; Yoon, Y.; Snyder, S.; Wert, E. *Environ. Sci. Technol.* **2005**, *39* (17), 6649−6663.

(8) Poole, A. J. *Water Res.* **2004**, *38* (14−15), 3458−3464.

(9) Gaya, U. I.; Abdullah, A. H. *J. Photochem. Photobiol., C* **2008**, *9* (1), 1−12.

(10) Saien, J.; Soleymani, A. R. *J. Hazard. Mater.* **2007**, *144* (1−2), 506−512.

(11) Robert, D.; Malato, S. *Sci. Total Environ.* **2002**, *291* (1−3), 85−97.

(12) Vione, D.; Maddigapu, P. R.; De Laurentiis, E.; Minella, M.; Pazzi, M.; Maurino, V.; Minero, C.; Kouras, S.; Richard, C. *Water Res.* **2011**, *45* (20), 6725−6736.

(13) Diebold, U. *Surf. Sci. Rep.* **2003**, *48* (5−8), 53−229.

(14) Gribb, A. A.; Banfield, J. F. *Am. Mineral.* **1997**, *82* (7−8), 717−728.

(15) Barnard, A. S.; Zapol, P. *Phys. Rev. B* **2004**, *70* (23), 235403.

(16) Cheng, H. M.; Ma, J. M.; Zhao, Z. G.; Qi, L. M. *Chem. Mater.* **1995**, *7* (4), 663−671.

(17) Mendez-Arriaga, F.; Esplugas, S.; Gimenez, J. *Water Res.* **2008**, *42* (3), 585−594.

(18) Ohno, T.; Tokieda, K.; Higashida, S.; Matsumura, M. *Appl. Catal., A* **2003**, *244* (2), 383−391.

(19) Lei, S.; Weng, D. *J. Environ. Sci.*−*China* **2008**, *20* (10), 1263−1267.

(20) Mansilla, H. D.; Bravo, C.; Ferreyra, R.; Litter, M. I.; Jardim, W. F.; Lizama, C.; Freer, J.; Fernandez, J. *J. Photochem. Photobiol., A* **2006**, *181* (2−3), 188−194.

(21) Linsebigler, A. L.; Lu, G.; Yates, J. T. *Chem. Rev.* **1995**, *95* (3), 735−758.

(22) Henderson, M. A. *Surf. Sci. Rep.* **2011**, *66* (6−7), 185−297.

(23) Jassby, D.; Farner Budarz, J.; Wiesner, M. *Environ. Sci. Technol.* **2012**, *46* (13), 6934−6941.

(24) Grzechulska, J.; Morawski, A. W. *Appl. Catal., B* **2002**, *36* (1), 45−51.

(25) Daneshvar, N.; Salari, D.; Khataee, A. R. *J. Photochem. Photobiol., A* **2003**, *157* (1), 111−116.

(26) Lachheb, H.; Puzenat, E.; Houas, A.; Ksibi, M.; Elaloui, E.; Guillard, C.; Herrmann, J.-M. *Appl. Catal., B* **2002**, *39* (1), 75−90.

(27) Suttiponparnit, K.; Jiang, J. K.; Sahu, M.; Suvachittanont, S.; Charinpanitkul, T.; Biswas, P. *Nanoscale Res. Lett.* **2011**, 6.

(28) Tschirch, J.; Dillert, R.; Bahnemann, D.; Proft, B.; Biedermann, A.; Goer, B. *Res. Chem. Intermed.* **2008**, *34* (4), 381−392.

(29) Sagara, T.; Iizuka, J.; Niki, K. *Langmuir* **1992**, *8* (3), 1018−1025.

(30) Dalrymple, O. K.; Yeh, D. H.; Trotz, M. A. *J. Chem. Technol. Biotechnol.* **2007**, *82* (2), 121−134.

(31) Kinsinger, N. M.; Wong, A.; Li, D.; Villalobos, F.; Kisailus, D. *Cryst. Growth Des.* **2010**, *10* (12), 5254−5261.

(32) Zhang, H. Z.; Banfield, J. F. *J. Mater. Res.* **2000**, *15* (2), 437−448.

(33) Ohno, T.; Sarukawa, K.; Matsumura, M. *New J. Chem.* **2002**, *26* (9), 1167−1170.

(34) Penn, R. L.; Banfield, J. F. *Geochim. Cosmochim. Acta* **1999**, *63* (10), 1549−1557.

(35) Huang, F.; Zhang, H.; Banfield, J. F. *J. Phys. Chem. B* **2003**, *107* (38), 10470−10475.

(36) Kosmulski, M. *Adv. Colloid Interface Sci.* **2009**, *152* (1−2), 14−25.

(37) Kosmulski, M. *J. Colloid Interface Sci.* **2009**, *337* (2), 439−448.

(38) Jiang, Y.; Sun, Q.; Jiang, Z.; Zhang, L.; Li, J.; Li, L.; Sun, X. *Mater. Sci. Eng.* **2009**, *29* (1), 328−334.

(39) Bullard, J. W.; Cima, M. J. *Langmuir* **2006**, *22* (24), 10264−10271.

(40) Kartha, S. S.; Chacko, C. E.; Bumpous, J. M.; Fleming, M.; Lentsch, E. J.; Flynn, M. B. *Otolaryngol.*−*Head Neck Surg.* **2006**, *135* (5), 765−768.

(41) Bach, K. K.; Lindsay, F. W.; Berg, L. S.; Howard, R. S. *Anesth. Analg.* **2004**, *99* (5), 1573−1574.

(42) Konstantinou, I. K.; Albanis, T. A. *Appl. Catal., B* **2004**, *49* (1), 1−14.

(43) Tschirch, J.; Bahnemann, D.; Wark, M.; Rathouský, J. *J. Photochem. Photobiol., A* **2008**, *194* (2−3), 181−188.

(44) Tschirch, J.; Dillert, R.; Bahnemann, D. *J. Adv. Oxid. Technol.* **2008**, *11* (2), 193−198.

(45) Houas, A.; Lachheb, H.; Ksibi, M.; Elaloui, E.; Guillard, C.; Herrmann, J. M. *Appl. Catal., B* **2001**, *31* (2), 145−157.

(46) Cong, S.; Xu, Y. M. *J. Phys. Chem. C* **2011**, *115* (43), 21161−21168.

(47) Liqiang, J.; Xiaojun, S.; Jing, S.; Weimin, C.; Zili, X.; Yaoguo, D.; Honggang, F. *Sol. Energy Mater. Sol. Cells* **2003**, *79* (2), 133−151.

(48) Torimoto, T.; Nakamura, N.; Ikeda, S.; Ohtani, B. *Phys. Chem. Chem. Phys.* **2002**, *4* (23), 5910−5914.

(49) Bickley, R. I.; Gonzalezcarreno, T.; Lees, J. S.; Palmisano, L.; Tilley, R. J. D. *J. Solid State Chem.* **1991**, *92* (1), 178−190.

(50) Hurum, D. C.; Agrios, A. G.; Gray, K. A.; Rajh, T.; Thurnauer, M. C. *J. Phys. Chem. B* **2003**, *107* (19), 4545−4549.

(51) Su, R.; Bechstein, R.; Sø, L.; Vang, R. T.; Sillassen, M.; Esbjörnsson, B.; Palmqvist, A.; Besenbacher, F. *J. Phys. Chem. C* **2011**, *115* (49), 24287−24292.

(52) Sun, B.; Vorontsov, A. V.; Smirniotis, P. G. *Langmuir* **2003**, *19* (8), 3151−3156.

(53) Carp, O.; Huisman, C. L.; Reller, A. *Prog. Solid State Chem.* **2004**, *32* (1−2), 33−177.

(54) Shi, F.; Li, Y.; Zhang, Q.; Wang, H. *J. Am. Ceram. Soc.* **2012**, *95* (6), 1927−1932.

(55) Liu, Z.; Zhang, X.; Nishimoto, S.; Jin, M.; Tryk, D. A.; Murakami, T.; Fujishima, A. *Langmuir* **2007**, *23* (22), 10916−10919.

(56) Murakami, N.; Kurihara, Y.; Tsubota, T.; Ohno, T. *J. Phys. Chem. C* **2009**, *113* (8), 3062−3069.

(57) Lin, H.; Huang, C. P.; Li, W.; Ni, C.; Shah, S. I.; Tseng, Y.-H. *Appl. Catal., B* **2006**, *68* (1−2), 1−11.

(58) Xu, Z.; Shang, J.; Liu, C.; Kang, C.; Guo, H.; Du, Y. *Mater. Sci. Eng., B* **1999**, *63* (3), 211−214.

(59) Nowotny, M. K.; Bahnemann, D. W. *Physica Status Solidi (RRL)* **2011**, *5* (3), 92−94.